Review

J. Mex. Chem. Soc. **2013**, *57(2)*, 144-157

ISSN 1870-249X

Cyclic C-F-Metal Containig Species. Solid State and Computational Examples

Maribel Arroyo Carranza[1] and Hugo Torrens Miquel[2]*

[1] Centro de Química del Instituto de Ciencias de la Benemérita Universidad Autónoma de Puebla. Edificio 103G del Complejo de Ciencias, Ciudad Universitaria, San Manuel, 72571, Puebla, Pue., Mexico. slmarroyo@hotmail.com

[2] División de Estudios de Posgrado, Facultad de Química, Universidad Nacional Autónoma de México, Ciudad. Universitaria, 04510 México D.F., México.
torrens@unam.mx

Received March 20, 2012; accepted April 16, 2013

Abstract. This article examines the results of research published between 2000 and 2012, which found experimental evidence of cyclic species containing the fragment carbon-fluorine-transition metal. 25 Examples (numbered throughout this paper) with 20 different metals and a wide variety of chemical environments have been gathered. A similar analysis brings together almost 40 transitional states and intermediates resulting from theoretical work studying the transition metal mediated carbon-fluorine bond activation. Among other aspects, this review is useful to recognize the specific characteristics which determine whether the C-F activation process is carried out through a concerted process, a mechanism assisted by auxiliary ligands or by free radicals.
Key words: Carbon, fluorine, bond activation, structure, theory.

Resumen. En este artículo se examinan los resultados de investigación publicados entre 2000 y 2012, en los que se han encontrado evidencias experimentales de especies cíclicas conteniendo al fragmento carbono-flúor-metal de transición. Se han reunido 25 ejemplos (numerados a lo largo de este trabajo) con 20 distintos metales y en una gran variedad de ambientes químicos. Un análisis similar reúne a casi 40 estados transicionales e intermediarios resultantes de trabajos teóricos enfocados al estudio de la activación del enlace carbono-flúor a través de metales de transición. Esta recopilación es de utilidad, entre otros aspectos, para reconocer las características específicas que determinan si el proceso de activación C-F se lleva a cabo mediante un proceso concertado, un mecanismo asistido por ligantes auxiliares o por radicales libres.
Palabras clave: Carbono, flúor, activación de enlace, estructura, teoría.

Introduction

The activation of the carbon-fluorine bond remains an area of great interest to those pursuing the replacement or removal of fluoride as well as to those who seek its incorporation into a given molecular structure. It is a process appealing to both, bond breakers and bond makers. The presence of cyclic species containing a carbon-fluorine-metal fragment has been repeatedly invoked as part of these processes either from a theoretical standpoint, as a result of kinetic studies or because the elusive carbon-fluorine-metal bonds have been observed in the solid state [1-8]. In this paper we gather some of these examples in each of these facets, although not in all cases the described metal containing cycles are directly involved in reactions promoting the activation of carbon-fluorine bonds.

Reviews focused on carbon-fluorine bond activation have been published [9] and a special issue of *Organometallics* has been dedicated to Fluorine in Organometallic Chemistry [10].

The compounds included in this review are grouped by metals and are described following the periodic table.

Scandium and Yttrium

In 2005, Bouwkamp *et al.* [11] studied the ionic metallocene complexes $[Cp^*_2M](BPh_4)$ ($Cp^* = C_5Me_5$) of the trivalent 3d metals Sc, Ti, and V. They found that for Sc, a complex of twelve electrons, the anion interacts weakly with the metal center through one of the phenyl groups. With Sc, these Lewis acidic species react with fluorobenzene and 1,2-difluorobenzene to yield $[Cp^*_2Sc(\kappa F\text{-}FC_6H_5)_2](BPh_4)$ and $[Cp^*_2Sc(\kappa^2F\text{-}1,2\text{-}F_2C_6H_4)](BPh_4)$ (**1**), the first examples of κF-fluorobenzene and κ^2F-1,2-difluorobenzene adducts of transition metals. With the perfluorinated anion $(B(C_6F_5)_4)^-$, Sc forms the $[Cp^*_2Sc(\kappa^2F\text{-}C_6F_5)B(C_6F_5)_3]$ (**2**) contact ion pair as shown in Figure 1. The nature of the metal-fluoroarene interaction was studied by density functional theory calculations and by comparison with the corresponding tetrahydrofuran adducts concluding that it is predominantly electrostatic.

Two years later, in 2007, Li *et al.* [12] synthesized the first cationic aminobenzyl-metal complex with a $(B(C_6F_5)_4)^-$ adduct as shown in Figure 2, $[(C_5Me_4SiMe_3)Sc(CH_2C_6H_4NMe_2\text{-}o)(\kappa^2F\text{-}C_6F_5)B(C_6F_5)_3]$ (**3**). An X-ray diffraction study revealed that compound **3** is a contact ion pair, in which the

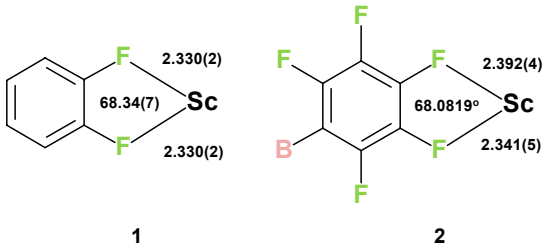

1 2

Fig. 1. Selected bond lengths (Å) and angles (°) in the metallocycle of $[Cp^*_2Sc(\kappa^2F\text{-}1,2\text{-}F_2C_6H_4)](BPh_4)$ (**1**) and $[Cp^*_2Sc(\kappa^2F\text{-}C_6F_5)B(C_6F_5)_3]$ (**2**) [11].

$(B(C_6F_5)_4)^-$ anion is coordinated to the metal center in a κ^2F-fashion with two adjacent (*ortho* and *meta*) F atoms (Fig. 3). Because of the higher electron deficiency of the cationic metal center in **3**, the bond distances of the Sc-$C_5Me_4SiMe_3$ bonds (av. 2.434(3)Å) are much shorter than those in its neutral precursor (av. 2.539(2)Å), and so are the Sc-benzyl (2.195(3)Å, precursor: 2.288(2)Å) and Sc-amino (2.300(3)Å, precursor: 2.470(2)Å) bond distances.

In a C_6D_5Cl solution, the four C_6F_5 groups in **3** showed one set of ^{19}F NMR signals, suggesting that it is a highly fluxional molecule, possibly due to the rapid dissociation and re-coordination of the $(B(C_6F_5)_4)^-$ unit or a solvent molecule. This fluxionality was not fixed even at −45 °C, as found in a variable-temperature ^{19}F NMR study.

Lara-Sanchez *et al.* [13] studied the reaction of $[Y(N(SiMe_3)_2)_3]$ with the fluorinated ligand (2-C_6F_5N=CH)(6-^{t}Bu)C_6H_3OH (HL) depicted in Figures 4 and 5. This reaction affords $[Y(N(SiMe_3)_2)(L)_2]$ (**4**) and $[Y(L)_3]$ (**5**). Both complexes are seven-coordinate in the solid state due to Y-F co-ordination to the C_6F_5 substituents.

Hayes *et al.* [14] isolated $[Y(\kappa F,\kappa C\text{-}C_6F_5)(C_6F_5)(THF)(ArNC_6H_4CHNAr)]$ (**6**), a six-coordinated Y compound containing a 4 membered cyclometallated ring, taking advantage from the fact that the precursor $[YPh_2((THF)(ArNC_6H_4CHNAr)]$, above –20 °C, undergo a C_6F_5 transfer process, ultimately yielding the bis-pentafluorophenyl derivative **6** and unidentified boron

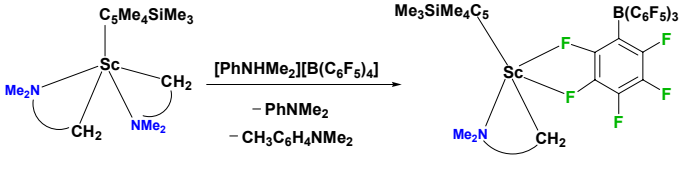

Fig. 2. Reaction leading to $[(C_5Me_4SiMe_3)Sc(CH_2C_6H_4NMe_2\text{-}o)(\kappa^2F\text{-}C_6F_5)B(C_6F_5)_3]$ (**3**) [12].

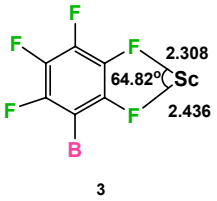

Fig. 3. Selected bond lengths (Å) and angles (°) in the metallocycle of $[(C_5Me_4SiMe_3)Sc(CH_2C_6H_4NMe_2\text{-}o)(\kappa^2F\text{-}C_6F_5)B(C_6F_5)_3]$ (**3**) [12].

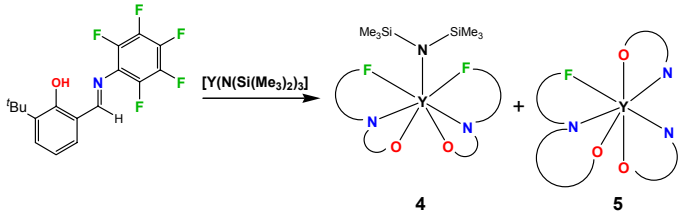

Fig. 4. Preparation of $[Y(N(SiMe_3)_2)(L)_2]$ (**4**) and $[Y(L)_3]$ (**5**) [13].

containing products. Compound **6** was isolated in low yield and identified by X-ray crystallography and features a distinct Y-F interaction involving one of the *ortho* F atoms in the solid state, as shown in Figures 6 and 7.

While exploring the coordination chemistry of the fluorinated diamino-dialkoxy tetradentate ligands $[OC(CF_3)_2CH_2N(Me)(CH_2)_nN(Me)CH_2C(CF_3)_2O]^{2-}$ (n = 2, $[ON^2NO]^{2-}$; n = 3, $[ON^3NO]^{2-}$) onto group 3 and group 4 metals, Lavanant and collaborators [15] found an efficient route to the yttrium complex $[Y(ON^2NO)(CH_2SiMe_3)(THF)]$ (**7**). X-ray crystallographic analysis reveals that this compound adopts in the solid state a seven-coordinate distorted structure, due to Y-F coordination to one of the four CF_3 substituents forming a 5-membered ring (Y-F 2.806(2) Å) as shown in Figure 8. In contrast, NMR studies show that it adopts a *C*2-symmetric structure in solution with no Y-F interaction.

Titanium, Zirconium and Hafnium

As mentioned above, Bouwkamp *et al.* [11] studied the ionic metallocene complexes $[Cp^*_2M](BPh_4)$ ($Cp^* = C_5Me_5$) of the

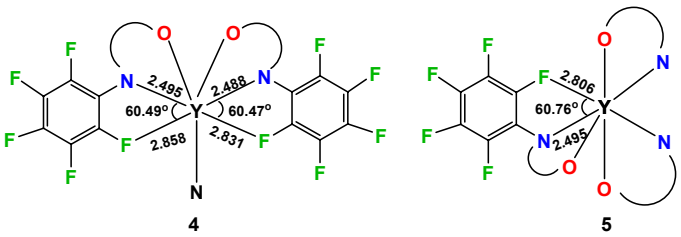

Fig. 5. Bond lengths (Å) and angles (°) in the metallocycles of $[Y(N(SiMe_3)_2)(L)_2]$ (**4**) and $[Y(L)_3]$ (**5**) [13].

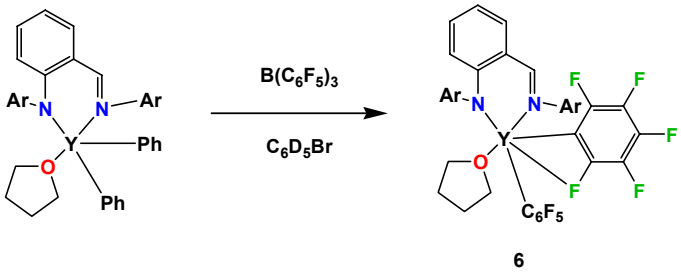

Fig. 6. Reaction leading to the synthesis of compound $[Y(\kappa F,\kappa C\text{-}C_6F_5)(C_6F_5)(THF)(ArNC_6H_4CHNAr)]$ (**6**) [14].

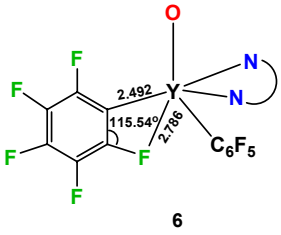

Fig. 7. Bond lengths (Å) and angles (°) in the metallocycle of $[Y(\kappa F,\kappa C\text{-}C_6F_5)(C_6F_5)(THF)(ArNC_6H_4CHNAr)]$ (**6**) [14].

trivalent 3d metals Sc, Ti, and V. They found that for M = Ti and V, the cations are naked. Crystallographic studies shown that they each contain one strongly distorted Cp* ligand, with two agostic C-H-Ti interactions involving the Me groups of Cp*. For Ti, these Lewis acidic species react with fluorobenzene and 1,2-difluorobenzene to yield $[Cp^*_2Ti(\kappa F\text{-}FC_6H_5)](BPh_4)$ and $[Cp^*_2Ti(\kappa^2F\text{-}1,2\text{-}F_2C_6H_4)](BPh_4)$ (**8**), the first examples of κF-fluorobenzene and κ^2F-1,2-difluorobenzene adducts of transition metals. With the perfluorinated anion $(B(C_6F_5)_4)^-$, Ti form a $[Cp^*_2Ti(\kappa^2F\text{-}C_6F_5)B(C_6F_5)_3]$ (**9**) contact ion pair (Fig. 9). The nature of the metal-fluoroarene interaction was studied by density functional theory calculations and by comparison with the corresponding tetrahydrofuran adducts and was found to be predominantly electrostatic for all metals studied.

Andino *et al.* [16] have studied the isomeric alkylidene complexes *syn*- and *anti*-[(PNP)Ti(=C^{t}Bu(C_6F_5))(F)] and [(PNP)Ti(=C^{t}Bu(C_7F_7))(F)], generated from C-F bond addition of hexafluorobenzene (C_6F_6) and octafluorotoluene (C_7F_8) by the alkylidyne ligand of the transient [(PNP)Ti≡C^{t}Bu], (PNP^- = N(2-P($CHMe_2$)$_2$-4-methylphenyl)$_2$).

Two mechanistic scenarios for the C-F bond activation of C_6F_6 are considered: 1,2-C-F addition of C_6F_6 to the fragment Ti≡C^{t}Bu to form (PNP)Ti≡C^{t}Bu(σ-C_6F_6) and [2+2]-cycloaddition of C_6F_6 to form the metallacyclobutene intermediate which undergo a β-fluoride elimination to yield 1-*syn*. Upon formation of the alkylidenes, the kinetic and thermodynamic alkylidene product is the *syn* isomer, which gradually isomerizes to the corresponding *anti* isomer to ultimately establish an equilibrium mixture (65/35) if the solution is heated in benzene to 105 °C for 1 h.

Single crystal X-Ray crystallographic data obtained for the *cis* and *trans* isomers are in good agreement with the computed DFT-optimized models shown in Figure 10 and 11.

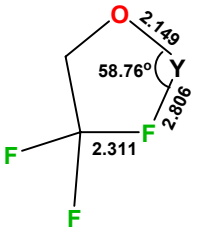

Fig. 8. Bond lengths (Å) and angles (°) in the carbon-fluorine-yttrium fragment of [Y(ON(CH_2)$_2$NO)(CH_2SiMe_3)(THF)] (**7**) [15].

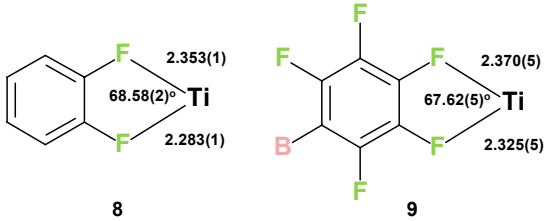

Fig. 9. Selected bond lengths (Å) and angles (°) in the metallocycle of $[Cp^*_2Ti(\kappa^2F\text{-}1,2\text{-}F_2C_6H_4)][BPh_4]$ (**8**) and $[Cp^*_2Ti(\kappa^2F\text{-}C_6F_5)B(C_6F_5)_3]$ (**9**) [11].

Wondimagegn and collaborators [17] have combined quantum mechanical and molecular mechanical models, to explore possible transformation routes for ion pair systems used as catalysts in olefin polymerization. The catalyst systems include $[(NPR_3)_2TiMe]^+(MeB(C_6F_5)_3)^-$, $[(Cp)(NCR_2)TiMe]^+(MeB(C_6F_5)_3)^-$, and $[(Cp)(SiMe_2NR)TiMe]^+(MeB(C_6F_5)_3)^-$ (Fig. 12). The possible thermal decomposition routes for the catalyst systems include fluorine transfer from $(MeB(C_6F_5)_3)^-$ to the metal center, aryl transfer (C_6F_5) to the growing chain, transfer

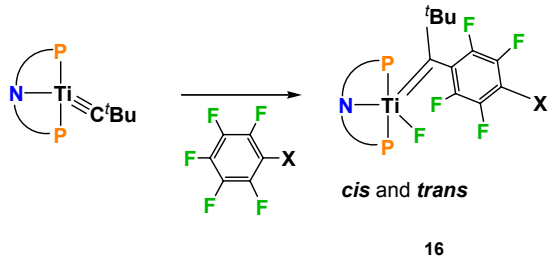

Fig. 10. Reaction scheme for the alkylidyne complex [(PNP)Ti≡C^{t}Bu] with C_6F_5X (X = F or CF_3) [16].

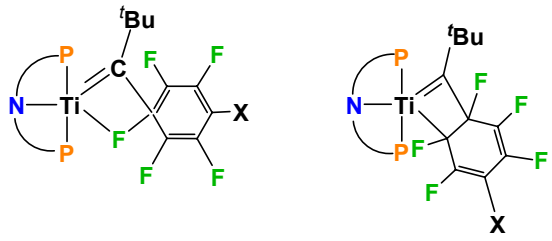

Fig. 11. Computed transition state in the 1,2-C-F addition and computed structure of the intermediate involved in the cycloaddition pathway leading to C-F activation [16]. Density Functional Theory as implemented in the Jaguar 7.0 suite of *ab initio* quantum chemistry programs. Geometry optimizations were performed with the B3LYP functional and the 6-31G** basis set. Transition metals were represented using the Los Alamos basis set (LACVP).

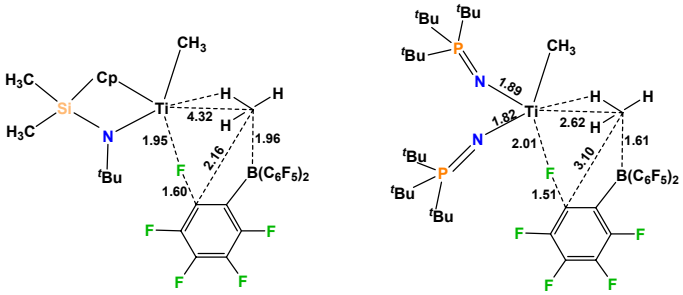

Fig. 12. Optimized transition states for fluoride transfer reactions (decomposition of the catalysts of olefin polymerization) involving the constrained geometry and the bis(phosphinimide) catalyst systems [17]. Density functional theory calculations were carried out using the Amsterdam Density Functional (ADF) program system, All calculations were based on the PW91 exchange-correlation functional.18 Combined quantum mechanical (QM) and molecular mechanical (MM) models were applied throughout. The MM atoms were described using the SYBYL/TRIPOS 5.2 force field constants.

of $B(C_6F_5)_3$ from $(MeB(C_6F_5)_3)^-$ to the ancillary ligand, exchange of methyl on butyl from the ancillary ligand with aryl in $(MeB(C_6F_5)_3)^-$, transfer of hydrogen from the Cp* ring to the growing chain, and transfer of hydrogen from the methyl group on tertiary butyl to the growing chain. The activation barriers fall in the range 15.5-68.7 kcal/mol. The transfer of fluorine from the counter ion to the metal center is the most facile deactivation pathway.

As part of their study of hetero bimetallic compounds, Gade and coworkers [18] determined the crystal structures of $[HC\{SiMe_2N(2,3,4\text{-}F_3C_6H_2)\}_3Zr(\mu\text{-}Cl)_2Li(OEt_2)_2]$ (**10**) and $[HC\{SiMe_2N(2\text{-}FC_6H_4)\}_3Zr(\mu\text{-}Cl)_2Li(OEt_2)_2]$ (**11**) in order to compare the role which the peripheral fluorine atoms play in both compounds. As in the monofluorophenyl analogue, the coordination at the central zirconium atom at **10** may be described, see Figure 13, as highly distorted octahedral with three amido-nitrogen atoms in facial sites, two bridging chloro ligands and with the sixth site being occupied by the *ortho*-fluorine atom of one of the phenyl groups. Considerable bonding character is indicated by the extent to which the phenyl ring is forced over to allow this chelate ring formation, giving a N-C-C intra-chelate angle of 114.6(4)° compared with 125.3(4)° for a non F bonded N-C-C angle.

Also, single-crystal X-ray structure analyses of $[HC\{SiMe_2N(2\text{-}FC_6H_4)\}_3Zr(\mu\text{-}CS_2)Fe(CO)_2Cp]$ (**12**) and $[HC\{SiMe_2N(2\text{-}FC_6H_4)\}_3Zr(\mu\text{-}SCNPh)Fe(CO)_2Cp]$ (**13**) were carried out. It is clear that the overall coordination of the zirconium atom in both **12** and **13** bears a striking resemblance to that found in the dichloride **10** and **11**.

As in the dichlorides, the tripodal ligands in the insertion products **12** and **13** both effectively occupy four coordination sites of the zirconium atom, with three facial nitrogen donors and an interaction from the *ortho*-fluoro atom of a peripheral phenyl ring at the fourth site. As in **11** the coordinating fluorophenyl ring is apparently being forced over to facilitate chelation [N-C-C 125.1(8)° and 124(1)° for the non F bonded rings, and N-C-C 114.8(8)° and 116(1)° for the F bonded rings in **12** and **13**, respectively]. In both dichlorides, the zirconium-nitrogen bond within the five membered chelate ring is the longest and that *trans* to the coordinating fluorine atom is the shortest. The shortening of the Zr-N(1) bond in each of these compounds is consistent with enhanced π donation from the amide donor *trans* to the highly electronegative fluorine atom. The persistence of the fluoro-zirconium interaction, from its presence in the starting material **10** to that in the heterodinuclear insertion products **12** and **13**, demonstrates the importance of the "active" ligand periphery in these compounds.

Giesbrecht and coworkers [19] have studied the compound $\{K(\eta^6\text{-}C_7H_8)_2\}\{ZrCl_2(N(C_6F_5)_2)_3\}$ (**14**) incorporating decafluorodiphenylamido ligands. The ^{19}F NMR spectrum of **14** reveals pentafluorophenyl resonances in a 2:1 ratio, consistent with a trigonal bipyramidal structure being maintained in solution. The crystal structure of **14** however, reveals a pseudo octahedral structure, with the sixth-coordination site being completed by a weak Zr-F interaction with a pentafluorophenyl group of an amido ligand as show in Figure 14.

Among the outstanding results from the group of Arndt *et al.* [20], there are a series of compounds containing cyclometallated rings resulting from F-Zr interactions. Besides suggested intermediate as [*rac*-(ebthi)Zr(η^2-$Me_3SiC_2SiMe_3$)] the crystal structure has been resolved for [(ebthi-(2-$BH(C_6F_5)_2$)Zr(κF-C_6F_5)] (**15**) (ebthi = 1,2-ethylene-1,1'-bis(η^5-tetrahydroindenyl)), Figure 15 and 16.

rac-(ebthi)Zr(η^2-$Me_3SiC_2SiMe_3$)] undergoes electrophilic substitution at one five-membered ring of the ebthi ligand upon reaction with $B(C_6F_5)_3$, forming the corresponding alkenyl complex **15**. In this complex, the boranate group is substituted at the 3-position of the five-membered ring, and one of its *ortho* fluorine atoms is coordinated to the zirconium center. The

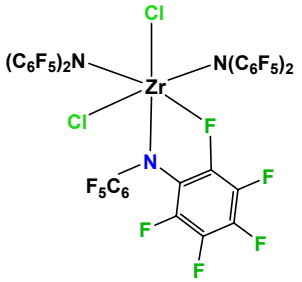

14

Fig. 14. A view of $[ZrCl_2(N(C_6F_5)_2)_3]^-$ (**14**) [19].

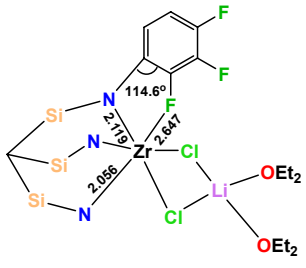

10

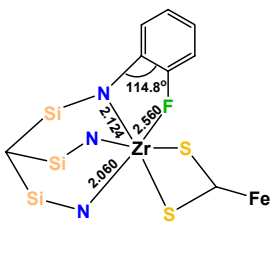

12

Fig. 13. Bond lengths (Å) and angles (°) in the metallocycle of $[HC\{SiMe_2N(2,3,4\text{-}F_3C_6H_2)\}_3Zr(\mu\text{-}Cl)_2Li(OEt_2)_2]$ **10** and $[HC\{SiMe_2N(2\text{-}FC_6H_4)\}_3Zr(\mu\text{-}CS_2)Fe(CO)_2Cp]$ **12** [18].

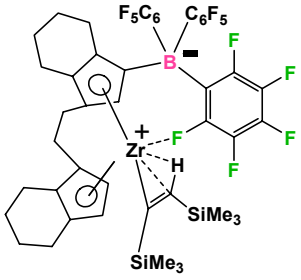

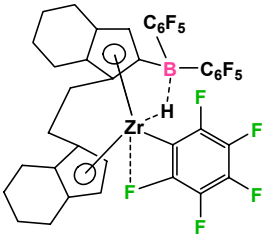

15

Fig. 15. Diagram of the suggested intermediate [(ebthi-(3-$B(C_6F_5)_2$(κF-C_6F_5)))Zr(η^2-$Me_3SiCCHSiMe_3$)] (left) and [(ebthi-(2-$BH(C_6F_5)_2$)Zr(κF-C_6F_5)] (**15**) [20].

σ-bound alkenyl group at the zirconium center participates in an additional agostic interaction.

Studying the bonding and bending in Zirconium(IV) and Hafnium(IV) hydrazides, Herrmann and collaborators [21] follow the reactions of the dichloro complexes [M($N_2^{TBS}N_{py}$)Cl_2] (M = Zr, Hf) with $LiNHNPh_2$ to afford mixtures of the two diastereomeric chlorohydrazido complexes [M($N_2^{TBS}N_{py}$)($NHNPh_2$)Cl] and also the reaction of [M($N_2^{TBS}N_{py}$)($NNPh_2$)(py)] with one molar equivalent of $B(C_6F_5)_3$ to give [Zr($N_2^{TBS}N_{py}$)(Ph_2NN{B(C_6F_5)$_2$(κF-C_6F_5)})] (**16**) and [Hf($N_2^{TBS}N_{py}$)(Ph_2NN{B(C_6F_5)$_2$(κF-C_6F_5)})] (**17**). In these products, $B(C_6F_5)_3$ becomes attached to the Nα atom of the side-on bound hydrazinediide and there is an additional interaction of an *ortho*-F atom of a C_6F_5 ring with the metal centre (Figs. 17 and 18).

In a work directed to evaluate the role of *ortho* halides in 1-hexene polymerization, Schrock *et al*. [22] determined by X-ray studies the structure of a series of compounds including the fluorinated, [Hf{(2,6-$F_2C_6H_3NCH_2$)$_2$C(CH_3)(2-C_5H_4N)}(^{i}Bu)$_2$] (**18**), with two fluorides weakly bonded to the metal as shown in Figure 19.

Activation of these type of complexes with (Ph_3C)($B(C_6F_5)_4$) in bromobenzene led to the formation of [Hf{(2,6-$X_2C_6H_3NCH_2$)$_2$C(CH_3)(2-C_5H_4N)}(^{i}Bu)][$B(C_6F_5)_4$) species that are also active for the polymerization of 1-hexene. The rate of consumption of 1-hexene followed a first-order dependence on 1-hexene (and hafnium), although the rates were substantially slower compared to those for the known catalyst with mesityl substituents on the amido nitrogens and slower when X = F than when X = Cl. The ease of preparation of the cations also followed the order aryl = mesityl > 2,6-$Cl_2C_6H_3$ > 2,6-$F_2C_6H_3$. Finally, the quality of the polymerization, in terms of its living characteristics, deteriorated markedly when the aryl was 2,6-$F_2C_6H_3$. In conclusion the introduction of *ortho* chlorides or fluorides decreases the rate of polymerization and also encourages β hydride elimination and formation of shorter polymer chains, therefore compromising the living characteristics of the polymerization.

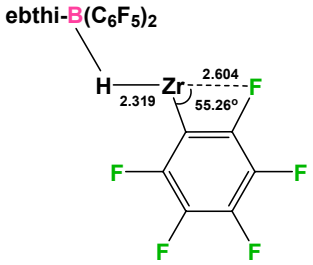

Fig. 16. Bond lengths (Å) and angles (°) in the zirconacycle of [(ebthi-(2-BH(C_6F_5)$_2$)Zr(κF-C_6F_5)] (**15**) [20].

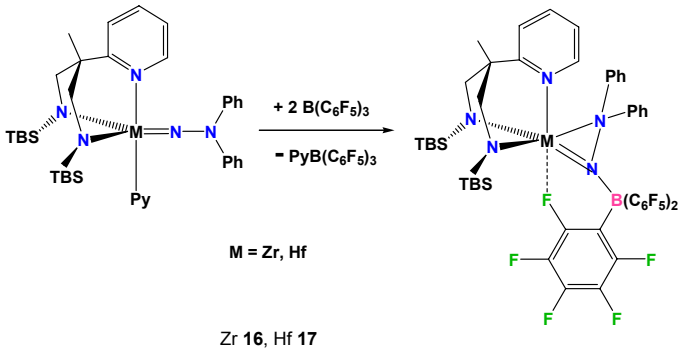

Fig. 17. Reaction scheme for the preparation of [Zr($N_2^{TBS}N_{py}$)(Ph_2NN{$B(C_6F_5)_2$(κF-C_6F_5)})] (**16**) and [Hf($N_2^{TBS}N_{py}$)(Ph_2NN{$B(C_6F_5)_2$(κF-C_6F_5)})] (**17**) [21].

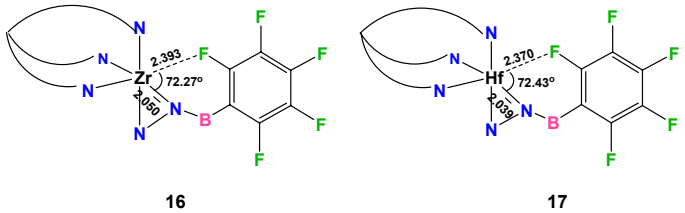

Fig. 18. Selected bond lengths (Å) and angles (°) in the metallocycle of [Zr($N_2^{TBS}N_{py}$)(Ph_2NN{$B(C_6F_5)_2$(κF-C_6F_5)})] (**16**) and [Hf($N_2^{TBS}N_{py}$)(Ph_2NN{$B(C_6F_5)_2$(κF-C_6F_5)})] (**17**) [21].

Vanadium

Giesbrecht *et al*. [19] have studied the interaction of VCl_3 with 3 equivalents of $KN(C_6F_5)_2$. This reaction generates the 'metallate' complex K[$VCl(N(C_6F_5)_2)_3$] (**19**); the solid state structure of **19** reveals a distorted trigonal bipyramid with the coordination sphere being completed by a weak V-F interaction with an *ortho*-fluorine of one of the decafluorodiphenylamido ligands as shown in Figure 20.

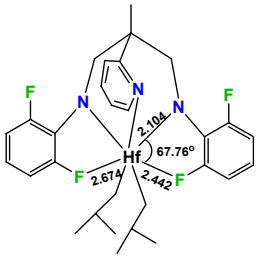

Fig. 19. Bond lengths (Å) and angles (°) in the metallocycle of [Hf{(2,6-$F_2C_6H_3NCH_2$)$_2$C(CH_3)(2-C_5H_4N)}(^{i}Bu)$_2$] (**18**) [22].

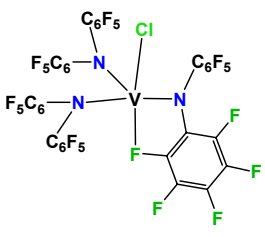

Fig. 20. A view of K{$VCl[N(C_6F_5)_2]_3$} (**19**) [19].

Molybdenum and Tungsten

Liu *et al*. [23] have found that monofluorinated benzenes undergo facile oxidative addition with the [W(HB($C_3H_3N_2$)$_3$)(NO)(PMe_3)] system, forming seven-coordinate aryl fluoride complexes. DFT calculations reveal two viable reaction pathways, one passing through a κF complex and one passing through an η^2-arene intermediate. From the κF complex, a modest 3 kcal/mol barrier is estimated to stand in the way of C-F activation, offering an explanation for the uncommonly rapid insertion of the metal. In contrast to reports of other second- or third-row transition metal complexes, C-H addition is not observed with monofluorinated benzenes, though this reaction is thought to be kinetically accessible. When the number of fluorines increases to four, C-H insertion becomes competitive, and for hexafluorobenzene or fluoronaphthalene, η^2-coordination dominates (Fig. 21).

Beltran and coworkers [24] have studied the catalytic hydrodefluorination (HDF) of pentafluoropyridine in the presence of arylsilanes which is catalyzed by the tungsten(IV) and molybdenum(IV) cluster hydrides of formula $[M_3S_4H_3(dmpe)_3]^+$, M = Mo or W (dmpe = 1,2-(bis)dimethylphosphinoethane). The reaction proceeds regioselectively at the 4-position under microwave radiation to yield the 2,3,5,6-tetrafluoropyridine.

A mechanism for the HDF reaction has been proposed that explains these results based on DFT calculations. The mechanism involves partial decoordination of the diphosphine ligand that generates an empty position in the metal coordination sphere. This position together with its neighbor M-H site are used to activate the C-F bond of the pentafluoropyridine through a M-H/C-F σ-bond metathesis mechanism involving a four-center transition state to give 2,3,5,6-tetrafluoropyridine. Subsequent coordination of the dangling diphosphine affords the *para*-substituted product and the fluoride cluster $[M_3S_4F_3(dmpe)_3]^+$, M = Mo or W, as seen in the following Figure 22.

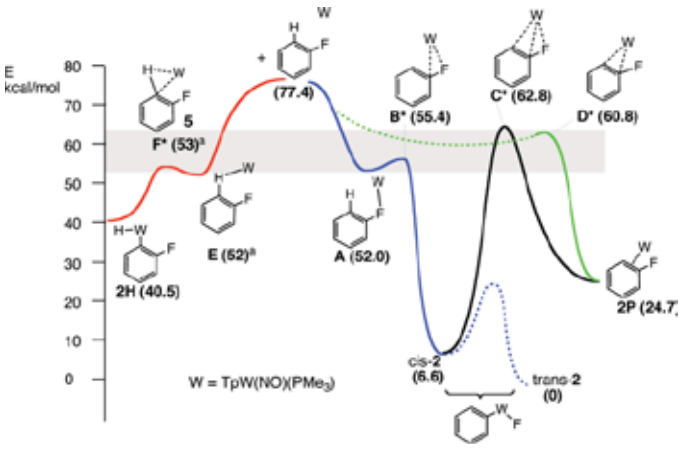

Fig. 21. Reaction coordinate diagram for C-F and C-H activation of fluorobenzene by [TpW(NO)(PMe_3)]. Density Functional Theory calculations using the Gaussian 03 program suite. Relative energies were determined using the LSDA density functional. The model incorporates the Los Alamos pseudopotential LANL2DZ and the associated basis functions. Reprinted with permission from reference 23. Copyright 2007. American Chemical Society.

Ruthenium and Osmium

Huang and coworkers [25] have found that the reactions of both [RuH(Ph)(CO)(P^tBu_2Me)$_2$] and [OsH(Ph)(CO)(P^tBu_2Me)$_2$] with vinyl fluoride readily form M-F bonds; however, Ru eliminates benzene, while Os eliminates ethylene. In contrast, [Ru(H)$_2$(CO)(P^tBu_2Me)$_2$] and [Os(H)$_2$(CO)(1-butene)(P^tBu_2Me)$_2$] both react with vinyl fluoride to give ethylene and [MHF(CO)(P^tBu_2Me)$_2$]. Ethylene production from both dihydrides is attributed to β-F migration to M from a four membered MCH_2CH_2F transient, Figure 23, while the unique behavior of [RuH(Ph)(CO)(P^tBu_2Me)$_2$] (giving the fluorine containig product [Ru(η^1-vinyl)F(CO)(P^tBu_2Me)$_2$] and benzene) is attributed to the difficulty of achieving ruthenium(IV), and the ability of the strongly π-acidic vinyl fluoride to rapidly trigger reductive elimination of benzene. The products of reaction of [RuH(Ar)(CO)(P^tBu_2Me)$_2$] with vinyl fluoride are redirected more towards ethylene formation when Ar carries fluorine substituents. The reaction products of [OsH(R)(CO)(P^tBu_2Me)$_2$] with vinyl fluoride revert to R-H elimination when R is methyl. Finally, the more π-acidic $H_2C{=}CF_2$ triggers very rapid CH_4 elimination from [OsH(CH_3)(CO)(P^tBu_2Me)$_2$]; cleavage of the second C-F bond yields the vinylidene [OsF$_2$(CCH_2)(CO)(P^tBu_2Me)$_2$].

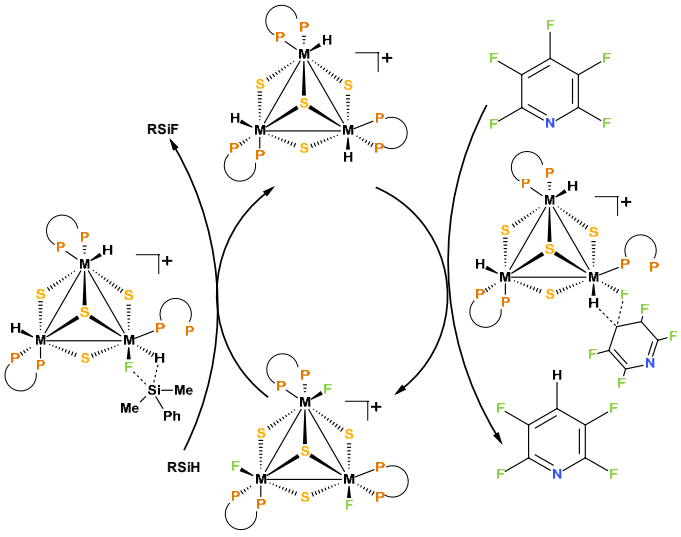

Fig. 22. Proposed mechanism for the HDF reaction with $[M_3S_4H_3(dmpe)_3]^+$, M = Mo or W, pentafluoropyridine and R_3SiH. Four-centered cycles with Si-F-M-H, and C-F-M-H are postulated. Density Functional Theory calculations were performed with the Gaussian03 package at the B3PW91 level. Transition metal atoms were represented by the relativistic effective core potential (RECP) from the Stuttgart group and its associated basis set, augmented by an f polarization function (Mo: R = 1.043; W: R=0.823). P, S, and Si atoms were represented by the relativistic effective core potential (RECP). Reprinted with permission from reference 24. Copyright 2011. American Chemical Society.

Ritter *et al*. [26] have described the synthesis, structure, and the activity of new ruthenium-based olefin metathesis catalysts featuring fluorinated *N*-heterocyclic carbene ligands [$RuCl_2$(carbene)(ligand)] (**20**).

The introduction of *ortho* halogen atoms profoundly alters the catalytic metathesis performance. Structural investigation suggested that an uncommon fluorine-ruthenium interaction, seen on Figure 24, is responsible for the significant rate enhancement. This is the first example of such an interaction resulting in increased catalytic activity.

Cobalt, rhodium and iridium

Giesbrecht *et al*. [19] found that CoI_2 reacts with 2 equivalents of. $NaN(C_6F_5)_2$ in the presence of pyridine to produce the expected product [Co{$N(C_6F_5)_2$}{$N(C_6F_5)(\kappa F\text{-}C_6F_5)$}$(py)_2$] (**21**); X-ray crystallography reveals a five-coordinate species in the solid state which is additionally stabilized by a weak Co-F interaction, Figure 25.

Dugan and coworkers [27] have studied the overall binuclear oxidative addition of fluorinated arenes to the cobalt(I) complex [$L^{t\text{Bu}}$Co] ($L^{t\text{Bu}}$ = 2,2,6,6-tetramethyl-3,5-bis(2,6-diisopropylphenylimido)-hept-4-yl) to give cobalt(II) complexes [$L^{t\text{-Bu}}$Co(μ-F)]$_2$ and [$L^{t\text{Bu}}$Co(Ar)], in a 1:2 molar ratio. The C-F activation reaction has a first-order rate dependence on both cobalt and fluorobenzene concentrations. The rate is increased by *meta*-fluoride substituents, and is slowed by *ortho*-fluoride substituents, suggesting electronic and steric influences on the transition state, respectively. The authors find that data are most consistent with a mechanism beginning with rate-limiting oxidative addition of the aryl fluoride to cobalt(I), followed by rapid reduction of the cobalt(III) aryl fluoride intermediate by a second molecule of [$L^{t\text{Bu}}$Co] (Fig. 26).

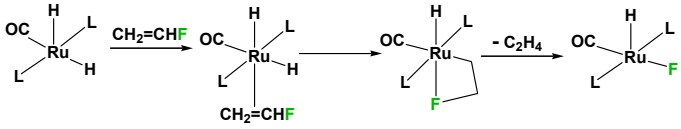

Fig. 23. Ethylene production from both [$MH_2(CO)L_2$] (M = Ru, Os; L = P^{t}Bu$_2$Me) is attributed to the insertion of vinyl fluoride into the M-H bond followed by β-F migration to M from a four membered MCH_2CH_2F transient species [25].

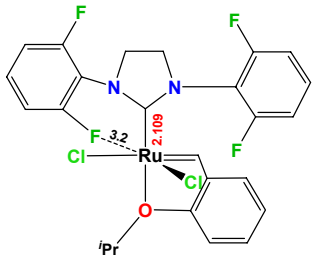

20

Fig. 24. Diagram of the Ru catalyst [$RuCl_2$(Carbene)(ligante)] (**20**) and bond lengths (Å) for the metallocycle Ru-F-C-C-N-C in **20** [26].

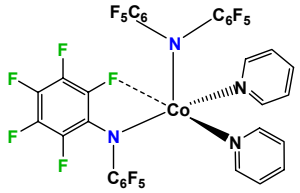

21

Fig. 25. A view of [Co{$N(C_6F_5)_2$}{$N(C_6F_5)(\kappa F\text{-}C_6F_5)$}$(py)_2$] (**21**) [19].

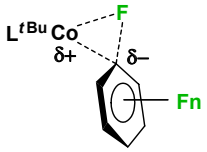

Fig. 26. Proposed transition state for C-F cleavage at Ar-F by [$L^{t\text{Bu}}$Co] [27].

In a remarkable paper, Erhardt and Macgregor [28] used density functional theory calculations to model the reaction of C_6F_6 with [$IrMe(PEt_3)_3$], this reaction proceeds with both C-F and P-C bond activation to yield *trans*-[$Ir(C_6F_5)(PEt_3)_2(PEt_2F)$], C_2H_4, and CH_4. Using a model species, *trans*-[$IrMe(PH_3)_2(PH_2Et)$], a low-energy mechanism involving nucleophilic attack of the electron-rich Ir metal center at C_6F_6 with displacement of fluoride has been identified. A novel feature of this process is the capture of fluoride by a phosphine ligand to generate a metallophosphorane intermediate [$Ir(C_6F_5)(Me)(PH_3)_2(PH_2EtF)$]. These events occur in a single step via a 4-centered transition state, in a process that has been termed "phosphine-assisted C-F activation". Alternative mechanisms based on C-F activation via concerted oxidative addition or electron-transfer processes proved less favorable. From the metallophosphorane intermediate the formation of the final products can be accounted for by facile ethyl group transfer from phosphorus to iridium followed by β-H elimination of ethene and reductive elimination of methane. The interpretation of phosphine-assisted C-F activation in terms of nucleophilic attack is supported by the reduced activation barriers computed with the more electron-rich model reactant *trans*-[$IrMe(PMe_3)_2(PMe_2Et)$] and the higher barriers found with lesser fluorinated arenes. Reactivity patterns for a range of fluoroarenes indicate the dominance of the presence of *ortho*-F substituents in promoting phosphine-assisted C-F activation, and an analysis of the charge distribution and transition state geometries indicates that this process is controlled by the strength of the Ir-aryl bond that is being formed (Fig. 27).

In a fundamental work, Choi and collaborators [29] have found the addition of C(sp^3)-F bonds to a pincer compound [(PCP)Ir(NBE)] (NBE = norbornene) via the initial, reversible cleavage of a C-H bond. One example is shown on Figure 28.

The results of density functional theory calculations, offer additional support for the proposed mechanism above. On the basis of the approximate reaction rates, the experimental free

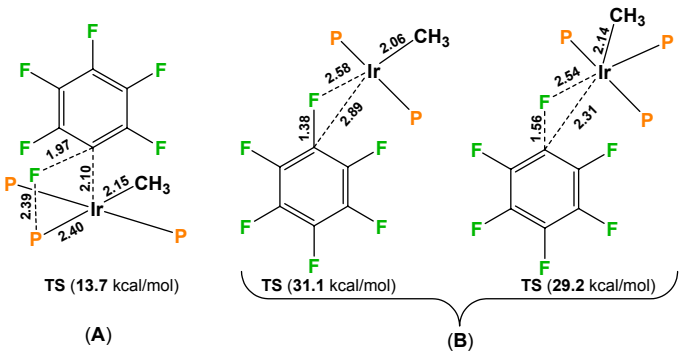

Fig. 27. For the interaction of C_6F_6 with the model *trans*-[IrMe(PH_3)$_2$(PH_2Et)], computed geometries for stationary points along: (A) the phosphine-assisted C-F activation mechanism and (B) the C-F oxidative addition mechanism, which proved less favoured [28]. Density Functional Theory calculations were run with Gaussian 0323a using the BP86 functional. The SSD pseudopotential and the associated basis set were used to described IR; 6-31G** basis sets were used for all other atoms.

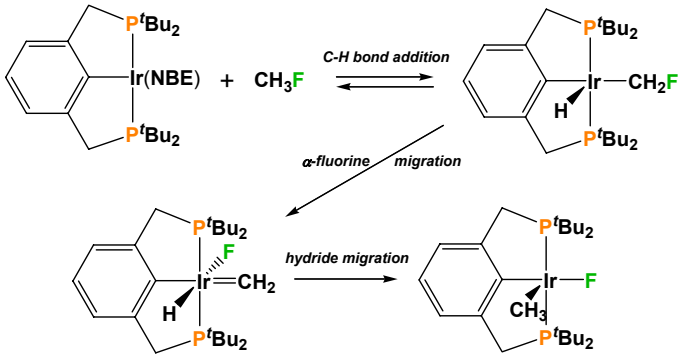

Fig. 28. Proposed mechanism on experimental bases for the oxidative addition of CH_3F to [(PCP)Ir(NBE)] complex [29].

energy barrier is about 23 kcal/mol. Direct addition of the C-F bond of CH_3F (i.e., addition via a three-centered transition state Ir-F-CH_3) is calculated to have a prohibitively high barrier ($\Delta G^{\ddagger}$ = 31.1 kcal/mol relative to the fragment (PCP)Ir or 37.5 kcal/mol relative to [(PCP)Ir(NBE)]). In contrast, the pathway depicted on Figure 28 is calculated to have a substantially lower barrier ($\Delta G^{\ddagger}$ = 16.5 kcal/mol relative to the fragment (PCP)Ir or 22.9 kcal/mol relative to [(PCP)Ir(NBE)]) fully consistent with the observed rate, attributable to the transition state of an α-fluorine-migration rate-determining step (three-centered transition state Ir-F-CH_2). Density Functional Theory calculations were performed using the *Gaussian09* collection of computer programs. Emploing the M06 model. For Ir, the Hay-Wadt relativistic effective and the LANL2TZ basis set were applied. Vibrational frequencies were employed to determine zero-point energy corrections.

Nickel, Palladium and Platinum

In an impressive work, Schaub and collaborators [30] have described the reaction of [Ni_2(^{i}Pr_2Im)$_4$(COD)] or [Ni(^{i}Pr_2Im)$_2$(η^2-C_2H_4)] (^{i}Pr_2Im = 1,3-di(*iso*propyl)imidazol-2-ylidene), with different fluorinated arenes. These reactions occur with a high chemo- and regioselectivity. In the case of polyfluorinated aromatics of the type C_6F_5X such as hexafluorobenzene, octafluorotoluene, trimethyl(pentafluorophenyl)silane, or decafluorobiphenyl, the C-F activation regioselectively takes place at the C-F bond in the *para* position to the X group to afford the complexes [Ni(^{i}Pr_2Im)$_2$(X)(C_6F_5)]. *trans*-[Ni(^{i}Pr_2Im)$_2$(F)(4-($SiMe_3$)C_6F_4)] was structurally characterized by X-ray diffraction.

The reaction of [Ni_2(^{i}Pr_2Im)$_4$(COD)] with partially fluorinated aromatic substrates $C_6H_xF_y$ leads to the products of a C-F activation, for example *trans*-[Ni(^{i}Pr_2Im)$_2$(F)(2-C_6FH_4)]. The reaction of [Ni_2(^{i}Pr_2Im)$_4$(COD)] with octafluoronaphthalene yields exclusively *trans*-[Ni(^{i}Pr_2Im)$_2$(F)(1,3,4,5,6,7,8-$C_{10}F_7$)], the product of an insertion into the C-F bond in the 2-position, whereas for the reaction of [Ni(^{i}Pr_2Im)$_2$(η^2-C_2H_4)] with octafluoronaphthalene two isomers are formed.

The reaction of [Ni_2(^{i}Pr_2Im)$_4$(COD)] or [Ni(^{i}Pr_2Im)$_2$(η^2-C_2H_4)] with pentafluoropyridine at low temperatures affords *trans*-[Ni(^{i}Pr_2Im)$_2$(F)(4-C_5NF_4)] as the sole product, whereas the reaction of [Ni(^{i}Pr_2Im)$_2$(η^2-C_2H_4)] performed at room temperature leads to the generation of *trans*-[Ni(^{i}Pr_2Im)$_2$(F)(4-C_5NF_4)] and *trans*-[Ni(^{i}Pr_2Im)$_2$(F)(2-C_5NF_4)].

The detection of intermediates as well as kinetic studies gives some insight into the mechanistic details for the activation of an aromatic carbon-fluorine bond at the {Ni(^{i}Pr_2Im)$_2$} complex fragment.

The intermediates of the reaction of [Ni(^{i}Pr_2Im)$_2$(η^2-C_2H_4)] with hexafluorobenzene and octafluoronaphthalene, [Ni(^{i}Pr_2Im)$_2$(η^2-C_6F_6)] and [Ni(^{i}Pr_2Im)$_2$(η^2-$C_{10}F_8$)], have been detected in solution. They convert into the C-F activation products.

Furthermore, density functional theory calculations on the reaction of [Ni_2(^{i}Pr_2Im)$_4$(COD)] with hexafluorobenzene, octafluoronaphthalene, octafluorotoluene, 1,2,4-trifluorobenzene, and 1,2,3-trifluorobenzene are presented. Several calculated C-F-Ni cyclic species are described on this work (Fig. 29).

In 2007, Yandulov and Tran [31], reported a computational analysis on C-F reductive elimination from aryl palladium(II) fluorides. They explored *N*-heterocyclic carbenes and phosphines as auxiliary ligands. Three-coordinate T-shaped geometry of [PdL(Ar)F] (L = NHC, PR_3) was shown to offer kinetics and thermodynamics of Ar-F elimination largely compatible with synthetic applications, whereas coordination of strong fourth ligands to Pd or association of hydrogen bond donors with F each caused pronounced stabilization of palladium(II) reactant and increased activation barrier beyond the practical range. Potential C-F reductive elimination from [Pd(PMe_3)(Ph)F] was computed. Yandulov's calculations predicted that in the related tricoordinate NHC complex [Pd(Me_2NHC)(Ph)F] reductive elimination of Ar-F is more facile for electron-withdrawing substituents, similar to related carbon-heteroatom reductive elimination reactions and nucleophilic aromatic substitution reactions as shown in Figures 30 and 31.

Decreasing donor ability of L promotes elimination kinetics via increasing driving force and *para*-substituents on Ar exert a sizable SNAr-type TS effect.

Synthesis and characterization of the novel [Pd(C_6H_4-4-NO_2)ArL(μ-F)]$_2$ (L = P(o-Tolyl)$_3$; P(t-Bu)$_3$) revealed stability of the fluoride-bridged dimer forms of the requisite [PdL(Ar)(F)] as the key remaining obstacle to Ar-F reductive elimination in practice.

In 2010, the first systematic mechanistic study of C-F reductive elimination reactions from aryl palladium(IV) fluoride complexes was reported by Furuya *et al*. [32], with particular focus on the C-F reductive elimination from the palladium(IV) compound [PdF(LN)(LN$_2$(SO$_2$)(NO$_2$))] pyridyl-sulfonamide stabilized cationic Pd(IV) fluoride shown below. The proposed mechanism for C-F reductive elimination is based on activation parameters, rate dependence on the polarity of the reaction medium, Hammett analysis, and DFT calculations.

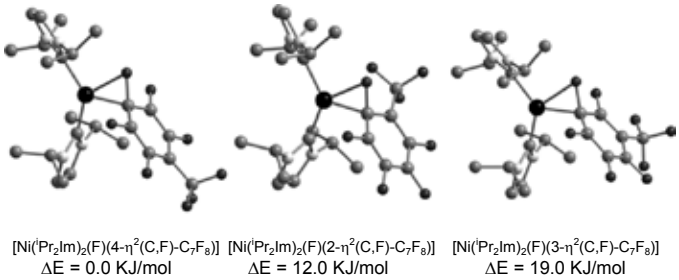

Fig. 29. Calculated structures and relative energies of likely transition states of the reaction of octafluorotoluene with the niquel derivatives [30]. Density Functional Theory calculations were run with of the TURBOMOLE program package, Version 5.7. For the DFT calculations the BP86 functional, SV(P) basis sets and the RI-J approximation were used. The equilibrium structures and transition states of the complexes were optimized at the RIDFT level using a SV(P) basis. Analytic second derivatives were calculated with the program AOFORCE using the RI-J approximation. All energies given are ZPE corrected.

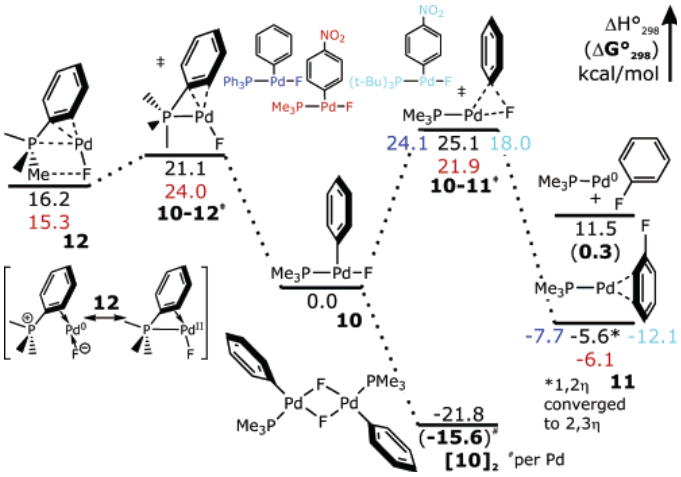

Fig. 31. Computed reactivity profile of [Pd(Ph)F(PMe$_3$)] and related analogs: [Pd(C_6H_4-4-NO_2)F(P(*t*-Bu)$_3$)] (numbers in cyan, right of center), [Pd(Ph)F(PPh$_3$)] (numbers in blue, left of center), and [Pd(C_6H_4-4-NO_2)F-(PMe$_3$)] (numbers in red, below center). Reprinted with permission from reference 31. Copyright 2007. American Chemical Society.

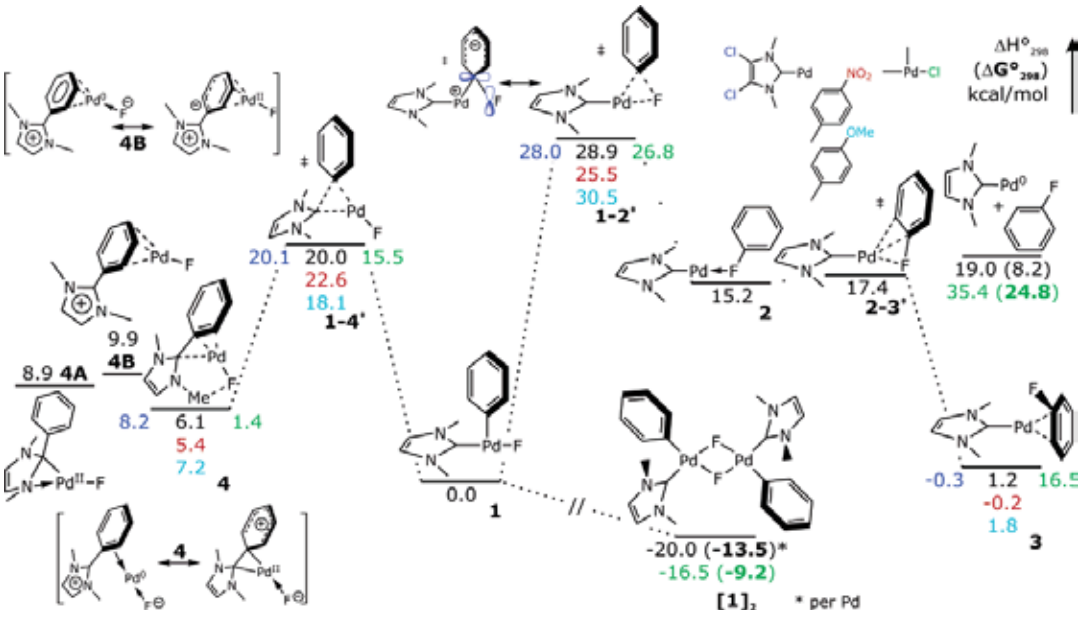

Fig. 30. Computed reactivity profile of [Pd(Ph)F(Me$_2$NHC)] and related analogs: [Pd(Ph)Cl(Me$_2$NHC)] (numbers in green, right of center or below), [Pd(Ph)F(4,5-Cl$_2$-Me$_2$NHC)] (numbers in blue, left of center), [Pd(C_6H_4-4-NO_2)F(Me$_2$NHC)] (numbers in red, below center), and [Pd(C_6H_4-4-OMe)F(Me$_2$NHC)] (numbers in cyan, second below center). Density Functional Theory calculations were carried out with Gaussian 03 suite of programs, using hybrid density functional method B3PW9167 for QM models. No symmetry constraints were imposed throughout with a single exception of [PdPh(Me$_2$NHC)(μ-Cl)]$_2$. All QM geometries were optimized under standard convergence criteria with BS I, which includes SDD quasirelativistic pseudopotentials. Reprinted with permission from reference 31. Copyright 2007. American Chemical Society.

The mechanistic study confirmed that C-F reductive elimination proceeds efficiently from aryl palladium(IV) fluoride complexes, supported by pyridyl-sulfonamide ancillary ligands. It was proposed that the pyridyl-sulfonamide ligand plays a crucial role for facile and efficient C-F bond formation. The ability of the pyridyl-sulfonamide ligand to function as a bidentate-tridentate-bidentate coordinating ligand during oxidation and reductive elimination, combined with the appropriate electronic requirements of the sulfonamide to position the aryl substituent *trans* to the sulfonamide ligand in the palladium(II) complex and the fluoride ligand *trans* to the sulfonamide ligand in the palladium(IV) complex, may be the reasons for facile C-F bond formation (Fig. 32).

Nova *et al*. [33] have examined the computed mechanisms for C-F bond activation at the 4-position of pentafluoropyridine by the model zero-valent bis-phosphine complex, [Pt(PH_3)(PH_2Me)]. Three distinct pathways leading to square-planar platinum(II) products are persistent. Direct oxidative addition leads to *cis*-[Pt(F)(4-C_5NF_4)(PH_3)(PH_2Me)] via a conventional 3-center transition state. This process competes with two different phosphine-assisted mechanisms in which C-F activation involves fluorine transfer to a phosphorus center via novel 4-center transition states. Figure 33. The more accessible of the two phosphine-assisted processes involves concerted transfer of an alkyl group from phosphorus to the metal to give a platinum(alkyl)(fluorophosphine) compound, *trans*-[Pt(Me)(4-C_5NF_3)(PH_3)(PH_2F)], analogues of which have been observed experimentally. The second phosphine assisted pathway sees fluorine transfer to one of the phosphine ligands with formation of a metastable metallophosphorane intermediate from which either alkyl or fluorine transfer to the metal is possible. Both Pt-fluoride and Pt(alkyl)(fluorophosphine) products are therefore accessible via this route. The calculation of Nova *et al*., Figures 33 and 34, highlight the central role of metallophosphorane species, either as intermediates or transition states, in aromatic C-F bond activation. In addition, the similar computed barriers for all three processes suggest that Pt-fluoride species should be accessible. This is confirmed experimentally by the reaction of [Pt(PR_3)$_2$] species (R = isopropyl (^{i}Pr), cyclohexyl (Cy), and

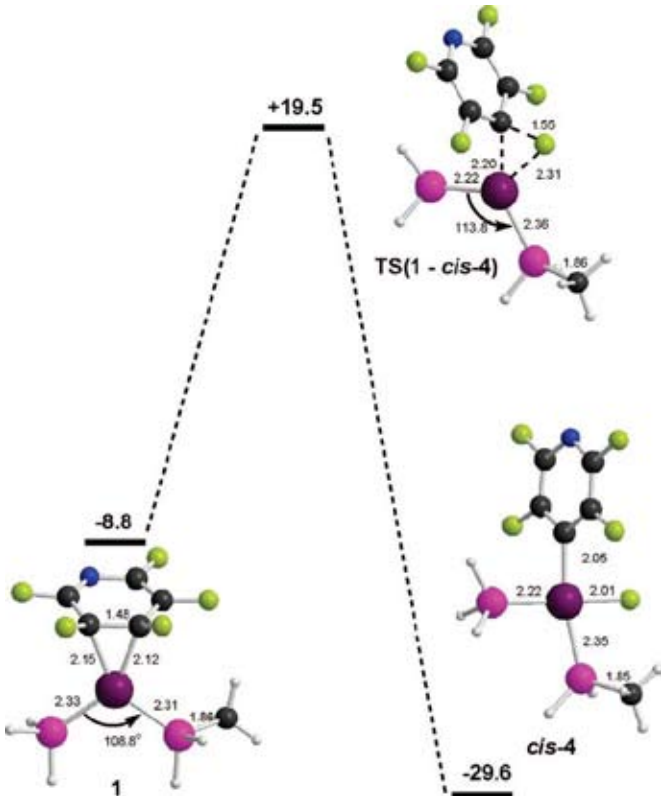

Fig. 33. Computed energy profile for C-F oxidative addition. Energies are relative to the isolated [Pt(PH_3)(PH_2Me)] and pentafluoropyridine reactants Energies are given in kcal/mol relative to the isolated reactants, and selected distances are in Å. Density Functional Theory calculations were performed using the Gaussian0337 package and employed the BP8638 functional. SDD pseudopotentials and the associated basis sets were used to describe Pt,39 while 6-31G(d,p) basis sets were used for all other atoms. Geometry optimizations were performed without symmetry constraints, and stationary points were characterized as minima or transition states by vibrational analysis. Transition states were further characterized by IRC calculations and subsequent geometry optimizations to confirm the nature of the minima involved in each step. All energies include a correction for zero-point energy. Reprinted with permission from reference 33. Copyright 2008. American Chemical Society.

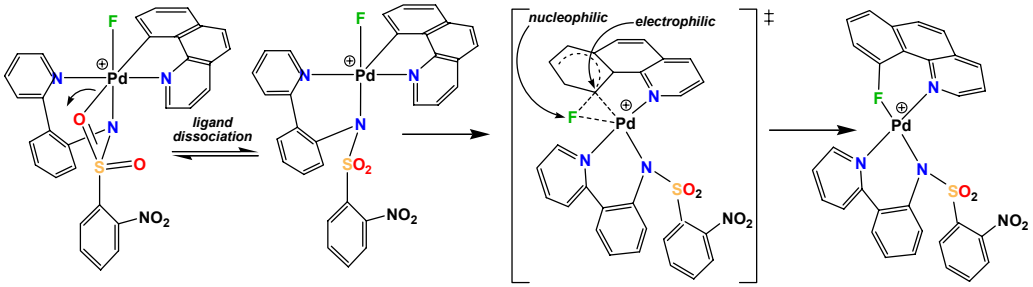

Fig. 32. Proposed mechanism for C-F reductive elimination from the Pd(IV) compound [PdF(LN)($LN_2(SO_2)(NO_2)$)] [32] Density Functional Theory calculations were performed using the M06 functional, as implemented in Jaguar 7.6 release. All calculations used the Hay and Wadt small core-valence relativistic effective-core-potential (ECP). The LACV3P** basis set was used for Pd and the 6-311G** basis set was used for F for all geometry optimizations and LACV3P++**(2f) and 6-311++G** basis sets for energies. LACV3P++**(2f) utilizes the LACV3P++** basis set as implemented in Jaguar plus a double-zeta f-shell with exponents from Martin and Sundermann. All electrons were described for all other atoms using the 6-31G** or 6-311++G** basis sets for geometry optimizations and energies.

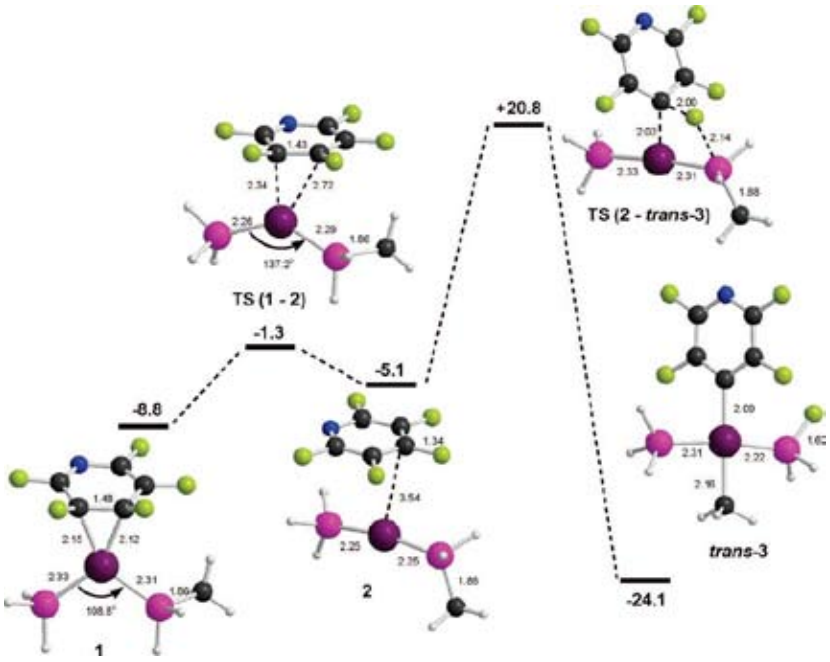

Fig. 34. Computed energy profile (kcal/mol) for phosphine-assisted C-F activation. Energies are relative to the isolated $[Pt(PH_3)(PH_2Me)]$ and pentafluoropyridine reactants, and selected distances are given in Å. Reprinted with permission from reference 33. Copyright 2008. American Chemical Society.

cyclopentyl (Cyp)) with 2,3,5-trifluoro-4-(trifluoromethyl)pyri dine to give *cis*-$[Pt(F)\{2\text{-}C_5NHF_2(CF_3)\}(PR_3)_2]$. These species subsequently convert to the *trans* isomers, either thermally or photochemically.

Moxey *et al.* [34] studied the reactions of a series of fluorinated bis(aryl)platinum(II) complexes, *cis*-$[Pt(Ar_F)_2(1,5\text{-}C_6H_{10})]$ (Ar_F = *p*-C_6HF_4, *p*-$C_6(OMe)F_4$ or $C_6H_2F_3$-2,4,6) with the four-membered gallium(I) or indium(I) heterocycles, $[E\{[N(Ar)]_2CN(C_6H_{11})_2\}]$ (E = Ga or In, Ar = $C_6H_3{}^iPr_2$-2,6) under various stoichiometries. These yielded either the 2:1 complexes, *cis*-$[Pt(Ar_F)_2\{Ga\{[N(Ar)]_2CN(C_6H_{11})_2\}\}_2]$, *trans*-$[Pt(C_6H_2F_3\text{-}2,4,6)_2\text{-}\{Ga\{[N(Ar)]_2CN(C_6H_{11})_2\}\}_2]$ and *trans*-$[Pt(Ar_F)_2\{In\{[N(Ar)]_2CN(C_6H_{11})_2\}\}_2]$, or the 3:1 complexes, *trans*-$[Pt(Ar_F)_2\{In\{[N(Ar)]_2CN(C_6H_{11})_2\}\}_3]$ (Ar_F = *p*-C_6HF_4 (**22**) or *p*-$C_6(OMe)F_4$ (**23**)), all of which were crystallographically characterized. The differing outcomes of these reactions are explained in terms of the lesser nucleophilicity and greater electrophilicity of the indium heterocycle relative to its gallium counterpart (Fig. 35). As show on Figure 36, in the solid state, the 3:1 indium complexes exhibit strong intramolecular In---F interactions which are indicative of their heterocyclic ligands displaying a "Lewis amphoteric" behaviour.

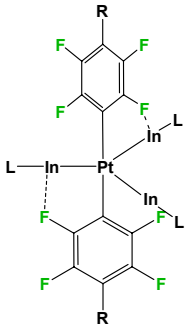

Fig. 35. Molecular structure of the 3:1 complexes, *trans*-$[Pt(Ar_F)_2\{In\{[N(C_6H_3{}^iPr_2\text{-}2,6)]_2CN(C_6H_{11})_2\}\}_3]$ (Ar_F = *p*-C_6HF_4 (**22**), In-F 2.501(2) (Å) or *p*-$C_6(OMe)F_4$ (**23**) IN-F 2.480(2) (Å)), all of which were crystallographically characterized [34].

Silver

Decken and coworkers [35] examined the synthetically useful solvent-free silver(I) salt $Ag[Al(pftb)_4]$ (pftb = $OC(CF_3)_3$). The salt was prepared by metathesis reaction of $Li[Al(pftb)_4]$ with $Ag[SbF_6]$ in liquid SO_2. The solvated complexes $[Ag(OSO)][Al(pftb)_4]$ (**24**), $[Ag(OSO)_2][SbF_6]$, and $[Ag(CH_2Cl_2)_2][SbF_6]$ were prepared and isolated by special techniques at low temperatures and structurally characterized by single-crystal X-ray diffraction. The SO_2 complexes provide the first examples of coordination of the very weak Lewis base SO_2 to silver(I).The SO_2 molecule in $[Ag(OSO)][Al(pftb)_4]$ is η^1-O coordinated to Ag^+, while the SO_2 ligands in $[Ag(OSO)_2][SbF_6]$ bridge two Ag^+ ions in an η^2-O,O' (*trans, trans*) manner.

Cadmium

Knapp and Mews [36] studied the ability of the sulfur-nitrogen-carbon bicycle $F_3CCN_5S_3$ to act as a donor towards transition metal cations. $F_3CCN_5S_3$ forms complexes with $[M(SO_2)_2](AsF_6)_2$ (M = Co, Cu, Zn, Cd) in the ratio 2:1 with the

composition $[M(F_3CCN_5S_3)_2(OSO)_2(FAsF_5)_2]$ (M = Co, Zn), $[Cu(F_3CCN_5S_3)_2(\mu\text{-}F)(\mu\text{-}F_2AsF_4)]_2$, and $[Cd(F_3CCN_5S_3)(\mu\text{-}F_3CCN_5S_3)(\eta^2\text{-}F_2AsF_4)_2]_2$ (**25**) in liquid sulfur dioxide.

The reaction with the larger and softer cadmium(II) cation results in a dinuclear complex that contains terminal and bridging $F_3CCN_5S_3$ ligands. Terminal ligands coordinates through the bridging nitrogen atom of $F_3CCN_5S_3$. Each bridging ligand coordinates two cadmium centers through two nitrogen atoms and, in addition, a third weak bonding interaction between one fluorine atom of the trifluoromethyl substituent and a cadmium(II) center is observed as shown in Figure 37. Bidentate hexafluoroarsenate ions complete the coordination sphere around the metal center, to give a coordination number of eight.

Final remarks

Across the periodic table a wide variety of transition metals are capable of forming the elusive carbon-fluorine-metal molecular fragment under the appropriate conditions. Table 1 shows the more relevant structural parameters —distances and angles— as well as elements on the cyclic fragment and their number. Whether these fragments will end up activating the

Table 1. Experimental evidence of cyclic species containing the fragment carbon-fluorine-transition mental.

#	COMPOUND	CYCLE	#C[1]	M-F(Å)	C-F(Å)	F-M-X (°)	C-F-M (°)	REF.
1	$[Cp^*_2Sc(\kappa^2F\text{-}1,2\text{-}F_2C_6H_4)](BPh_4)$	Sc-F-C=C-F-	5	2.330(2)	1.389(4)	68.34(7)	119.1(2)	11
		Sc-F-C=C-F-	5	2.330(2)	1.396(4)		118.8(2)	
2	$[Cp^*_2Sc(\kappa^2F\text{-}C_6F_5)B(C_6F_5)_3]$	Sc-F-C=C-F-	5	2.392(4)	1.377(7)	68.0(1)	116.3(3)	11
		Sc-F-C=C-F-	5	2.341(3)	1.383(7)		114.6(3)	
3	$[(C_5Me_4SiMe_3)Sc(CH_2C_6H_4NMe_2\text{-}o)(\kappa^2F\text{-}C_6F_5)B(C_6F_5)_3]$	Sc-F-C-C-F-	5	2.436(2)	1.385(3)	64.82(6)	117.32(17)	12
		Sc-F-C-C-F-	5	2.308(2)	1.382(3)		118.36(17)	
4	$[Y(N(SiMe_3)_2)(L)_2]$[2]	Y-F-C=C-N-	5	2.831(2)	1.349(5)	60.50(9)	109.1(2)	13
		Y-F-C=C-N-	5	2.858(2)	1.357(5)	60.47(9)	109.5(2)	
5	$[Y(L)_3]$[2]	Y-F-C=C-N-	5	2.806(2)	1.352(4)	60.76(9)	111.4(2)	13
6	$[Y(\kappa F,\kappa C\text{-}C_6F_5)(C_6F_5)(THF)(ArNC_6H_4CHNAr)]$	Y-F-C=C-	4	2.786(2)	1.376(4)	58.76(9)	89.74(17)	14
7	$[Y(ON(CH_2)_2NO)(CH_2SiMe_3)(THF)]$	Y-F-C=C-O-	5	2.811(3)	1.370(9)	69.48(9)	110.4(4)	15
8	$[Cp^*_2Ti(\kappa^2F\text{-}1,2\text{-}F_2C_6H_4)](BPh_4)$	Ti-F-C=C-F-	5	2.353(1)	1.378(2)	68.58(5)	117.8(1)	11
		Ti-F-C=C-F-	5	2.283(1)	1.383(3)		120.2(1)	
9	$[Cp^*_2Ti(\kappa^2F\text{-}C_6F_5)B(C_6F_5)_3]$	Ti-F-C=C-F-	5	2.325(5)	1.37(1)	67.6(2)	117.6(5)	11
		Ti-F-C=C-F-	5	2.370(5)	1.346(9)		115.4(5)	
10	$[HC\{SiMe_2N(2,3,4\text{-}F_3C_6H_2)\}_3Zr(\mu\text{-}Cl)_2Li(OEt_2)_2]$	Zr-F-C=C-N-	5	2.647(5)	1.315(6)	67.39(19)	106.5(3)	18
11	$[HC\{SiMe_2N(2\text{-}FC_6H_4)\}_3Zr(\mu\text{-}Cl)_2Li(OEt_2)_2]$	Zr-F-C=C-N-	5	2.647(5)	1.312(6)	67.4(5)	107.5(4)	18
12	$[HC\{SiMe_2N(2\text{-}FC_6H_4)\}_3Zr(\mu\text{-}CS_2)Fe(CO)_2Cp]$	Zr-F-C=C-N-	5	2.553(8)	1.324(7)	67.6(3)	109.7(6)	18
13	$[HC\{SiMe_2N(2\text{-}FC_6H_4)\}_3Zr(\mu\text{-}SCNPh)Fe(CO)_2Cp]$	Zr-F-C=C-N-	5	2.703(11	1.322(17)	66.9(4)	105.7(8)	18
14	$\{K(\eta^6\text{-}C_7H_8)_2\}\{ZrCl_2(N(C_6F_5)_3\}$	Zr-F-C=C-N-	5	2.602(2)	1.356(4)	67.94(8)	107.12(18)	19
15	$[(ebthi\text{-}(2\text{-}BH(C_6F_5)_2)Zr(\kappa F\text{-}C_6F_5)]$[3]	Zr-C=C-F-	4	2.604(5)	1.389(8)	55.3(2)	88.5(4)	20
16	$[Zr(N_2{}^{TBS}N_{py})(Ph_2NN\{B(C_6F_5)_2(\kappa F\text{-}C_6F_5)\})]$	Zr-F-C=C-B-N=	6	2.3930(13)	1.385(3)	72.27(6)	137.97(13)	21
17	$[Hf(N_2{}^{TBS}N_{py})(Ph_2NN\{B(C_6F_5)_2(\kappa F\text{-}C_6F_5)\})]$	Hf-F-C=C-B-N=	6	2.3704(12)	1.379(2)	72.43(5)	138.07(12)	21
18	$[Hf\{(2,6\text{-}F_2C_6H_3NCH_2)_2C(CH_3)(2\text{-}C_5H_4N)\}(^tBu)_2]$	(Hf-F-C=C-N-)C-	5	2.674(3)	1.386(5)	65.22(11)	108.7(2)	22
		(Hf-F-C=C-N-)C-	5	2.443(3)	1.366(5)	67.76(13)	114.5(3)	
19	$K[VCl(N(C_6F_5)_2)_3]$	V-F-C=C-N-	5	2.284(2)	1.373(4)	76.83(10)	109.3(2)	19
20	$[RuCl_2(Carbene)(L)]$[4]	Ru-F-C=C-N-C-	6	2.675(1)	1.355(2)	77.57(2)	111.31(3)	26
21	$[Co(N(C_6F_5)_2)\{N(C_6F_5)(\kappa F\text{-}C_6F_5)\}(py)_2]$	Co-F-C=C-N-	5	2.507(2)	1.365(5)	73.57(11)	106.1(2)	19
22	*trans*-$[Pt(p\text{-}C_6HF_4)_2\{In\{[N(Ar)]_2CN(C_6H_{11})_2\}\}_3]$	Pt-C=C-F-In-	5	2.501(2)	1.378(1)	84.25(3)	115.20(2)	34
		Pt-C=C-F-In-	5	2.501(2)	1.378(1)	84.25(3)	115.20(2)	
23	*trans*-$[Pt(p\text{-}C_6(OMe)F_4)_2\{In\{[N(Ar)]_2CN(C_6H_{11})_2\}\}_3]$	Pt-C=C-F-In-	5	2.480(2)	1.380(3)	84.81(4)	115.38(3)	34
		Pt-C=C-F-In-	5	2.480(2)	1.380(3)	84.81(4)4	115.38(3)	
24	$[Ag(OSO)][Al(pftb)_4]$[5]	Ag-F-C-C-O-	5	2.622(4)	1.27(2)	61.8(1)	120.5(8)	35
		Ag-F-C-C-O-	5	2.640(5)	1.29(1)	64.1(2)	107.2(6)	
		Ag-F-C-C-O-Al-O-	7	2.603(7)	1.35(1)	85.7(2)	148.7(5)	
25	$[Cd(F_3CCN_5S_3)(\mu\text{-}F_3CCN_5S_3)(\eta^2\text{-}F_2AsF_4)_2]_2$	Cd-F-C-C-N-	5	2.671(1)	1.349(3)	63.51(5)	115.56(1)	36

[1]number of members on the cycle.
[2]L = 2-(C_6F_5N=CH)-6-(^{t}Bu)$C_6H_3O^-$.
[3]ebthi = 1,2-ethylene-1,1'-bis(η^5-tetrahydroindenyl).
[4]Carbene = *N,N'*-(1,3-$F_2C_6H_3$-2-yl)$_2$(1,3-$N_2C_3H_4$-2-yl); L = =CH-C_6H_4-2-O-^{i}Pr.
[5]pftb = -OC(CF3)3.

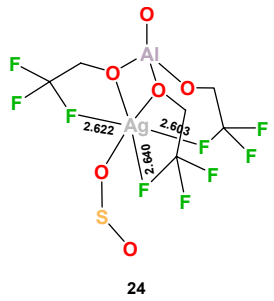

24

Fig. 36. Some selected bond lengths (Å) in the metallocycles of $[Ag(OSO)][Al(OC(CF_3)_3)_4]$ (**24**) [35].

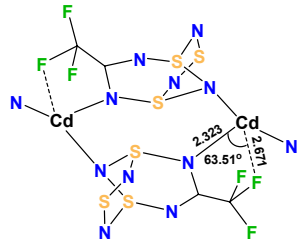

25

Fig. 37. Selected bond lengths (Å) and angles (°) in the metallocycle of $[Cd(F_3CCN_5S_3)(\mu\text{-}F_3CCN_5S_3)(\eta^2\text{-}F_2AsF_4)_2]_2$ (**25**) [36].

carbon fluorine bond either under a catalytic or stoichiometric regime, generally depends on very subtle experimental details. On the other hand, as expected, elegant and powerful theoretical calculations have shown new insights and pointed towards new targets on this area fueling the synergic experimental-theoretical research loop.

A broad picture would show that the driving forces behind the chemistry of the carbon-fluorine-metal bonds comes either from radical species, concerted oxidative addition, reductive elimination, fluorine substitution, ancillary ligand participation or a combination of these reaction mechanisms.

In general, the fluoride affinity of the highly electrophilic early transition metals tends to preclude their use in catalysis and the work described here for the metals of groups 3 to 5 show this tendency. Accordingly, the search for further developments has been directed to the use of low valent electron-rich transition metals.

As for ancillary ligand participation, several experiments result in relatively stable structures with the carbon-fluorine-metal bond originating from the ligand whereas calculations have shown that a phosphine-assisted C-F activation mechanism is possible with electron-rich precursors. The barrier associated with the phosphine-assisted process seems to be however, very similar to that for conventional oxidative addition and the balance between these processes is extremely delicate.

Several ligand based systems show promise and should be further studied as model compounds for systematic studies directed toward catalytic C-F bond activation processes.

From this work it is evident that significant progress has consistently been made in the area of metal-assisted C-F bond activation, early efforts typically employed forcing conditions and obtained low yields. C-F activation can now be accomplished under extremely mild conditions using a suitable transition-metal complex. However, considering the examples described in this paper, undoubtedly, the next challenge appears to be the activation of saturated perfluorocarbons and future efforts ought to profit from improved C-F bond cleavage processes directed toward the ultimate functionalization of the C-F bond.

Acknowledgement

We are grateful to DGAPA-UNAM-IN217611, to CONACYT-177498 and VIEP (ARCS-NAT-12-G) for support.

References

1. O'Hagan, D. *Chem. Soc. Rev.* **2008**, *37*, 308-319.
2. Clot, E.; Megret, C.; Eisenstein, O; Perutz, R. N. *J. Am. Chem. Soc***. 2009**, *131*, 7817-7827.
3. Furuya,T.; Klein, J.E.M.N.; Ritter T. *Synth.* **2010**, *11*, 1804-1821.
4. Clot, E.; Eisenstein, O.; Jasim, MacGregor, N. S.; McGrady, J. E.; Perutz R. N. *Acc. Chem. Res*. **2011**, *44*, 333-348.
5. Sun, A. D.; Love, J. A. *Dalton Trans.* **2010**, *39*, 10362-10374.
6. Partyka, D. V. *Chem. Rev*. **2011**, *111*, 1529-1595.
7. Crespo, M. *Organometallics* **2012**, *31*, 1216-1234.
8. Nova, A.; Mas-Balleste, R.; Lledos, A. *Organometallics* **2012**, *31*, 1245-1256.
9. a) Kiplinger, J. L.; Richmond T. G. and Osterberg, C. E. *Chem. Rev.* 1994, *94*, 373-431. b) Torrens H.; *Coord. Chem. Rev.*, 2005, *249*, 1957-1985. c) Perutz, R. N. and Braun, T.Transition Metal-mediated C-F Bond Activation. In *Comprehensive Organometallic Chemistry III*, d) Crabtree R. H. and Mingos, M. P. ed., Elsevier, Oxford, England, 2007; pp 725-758. e) Meike Reinhold, M.; McGrady, J. E.; and Perutz R. N. *J. Amer. Chem. Soc.* 2004, *126*, 5268-5276.
10. Special Issue: Fluorine in Organometallic Chemistry. Organometallics. Special issue Published February 27, 2012.
11. Bouwkamp, M. W.; Budzelaar, P. H. M.; Gercama, J.; Del Hierro Morales, I.; de Wolf, J.; Meetsma, A.; Troyanov, S. I.; Teuben, J. H.; Hessen, B. *J. Amer. Chem. Soc*. **2005**, *127*, 14310-14319.
12. Li, X.; Nishiura, M.; Mori, K.; Mashiko, T.; Hou, Z. *Chem. Commun*. **2007**, 4137-4139.
13. Lara-Sanchez, A.; Rodriguez A.; Hughes D.L.; Schormann M.; Bochmann M., *J. Organomet. Chem*. **2002**, *663,* 63-69.
14. Hayes, P.G.; Welch G. C.; H. Emslie D. J.; Noack C. L.; Piers W. E.; Parvez M. *Organometallics* **2003,** *22,* 1577-1579.
15. Lavanant, L.; Chou, T. Y.; Chi, Y.; Lehmann, C. W.; Toupet, L.; Carpentier, J. F. *Organometallics* **2004,** *23,* 5450-5458.
16. Andino, J. G.; Fan, H.; Fout, A. R.; Bailey, B. C.; Baik, M-H.; Mindiola, D. J. *J. Organomet. Chem*. **2011**, *696*, 4138-4146.
17. Wondimagegn, T.; Xu, Z.; Vanka, K.; Ziegler, T. *Organometallics* **2005,** *24,* 2076-2085.
18. Gade, L. H.; Memmler, H.; Kauper, U.; Schneider, A.; Fabre, S.; Bezougli, I.; Galka, M. L. C.; Scowen, I. J.; McPartlin, M. *Chem. Eur. J*. **2000**, *6*, 692-708.
19. Giesbrecht, G. R.; Gordon, J. C.; Clark, D. L.; Hijar, C. A.; Scott, B. L.; Watkin, J. G., *Polyhedron* **2003**, *22*,153-163.
20. a) Arndt, P.; Jager-Fiedler, U.; Klahn, M.; Baumann, W.; Spannenberg, Aa; Burlakov, V. V.; Rosenthal, U. *Angew. Chem. Int. Ed.* **2006**, *45*, 4195-4198. b) Arndt, P.; Baumann, W.; Spannenberg,

A.; Rosenthal, U.; Burlakov, V. V.; Shur, V. B. *Angew. Chem. Int. Ed*. **2003**, *42,* 1414-1418.
21. Herrmann, H.; Lloret Fillol, J.; Gehrmann, T.; Enders, M.; Wadepohl, H.; Gade, L. H. *Chem. Eur. J*. **2008**, *14*, 8131-8146.
22. Schrock, R. R.; Adamchuk, J.; Ruhland, K.; Pia L; Lopez H. *Organometallics* **2003,** *22,* 5079-5091.
23. Liu, W.; Welch, K.; Trindle, C. O.; Sabat, M.; Myers, W. H.; Harman, W. D. *Organometallics*, **2007**, *26*, 2589-2597.
24. Beltran, T. F, Feliz, M.; Llusar, R.; Mata, J. A.; Safont, V. S. *Organometallics* **2011**, *30*, 290-297.
25. Huang, D.; Renkema, K. B.; Caulton, K. G. *Polyhedron* **2006**, *25*, 459-468.
26. Ritter, T.; Day, M. W.; Grubbs, R. H. *J. Am. Chem. Soc*. **2006**, *128*, 11768-11769.
27. Dugan, T. R.; Goldberg, J. M.; Brennessel, W. W.;Holland, P. L. *Organometallics* **2012**, *31*, 1349-1360.
28. Erhardt, S.; Macgregor, S. A. *J. Am. Chem. Soc*. **2008**, *130*, 15490-15498.
29. Choi, J.; Wang, D. Y.; Kundu, S.; Choliy, Y.; Emge, T. J.; Krogh-Jespersen, K.; Goldman, A. S. ***Science*** **2011**, *332,* 1545-1548.
30. Schaub, T.; Fischer, P.; Steffen, A.; Braun, T.; Radius, U.; Mix, A. *J. Am. Chem. Soc*. **2008**, *130*, 9304-9317.
31. Yandulov, D. V. Tran, N. T. *J. Am. Chem. Soc.*, **2007**, *129*, 1342-1358.
32. Furuya, T.; Benitez, D.; Tkatchouk, E.; Strom, A. E.; Tang, P.; Goddard, W. A. III, Ritter, T. *J. Am. Chem. Soc*. **2010**, *132*, 3793-3807.
33. Nova, A.; Erhardt, S.; Jasim, N. A.; Perutz, R. N.; Macgregor, S. A.; McGrady, J. E.; Whitwood, A. C. *J. Am. Chem. Soc.* **2008**, *130*, 15499-15511.
34. Moxey, G. J.; Jones, C.; Stasch, A.; Junk, P. C.; Deacon, G. B.; Woodul W. D.; Drago P. R. *Dalton Trans.*, 2009, 2630-2636.
35. Decken, A.; Knapp, C.; Nikiforov, G. B.; Passmore, J.; Rautiainen, J. M.; Wang, X.; Zeng, X. *Chem.-Eur.J.* **2009**, *15*, 6504-6517.
36. Knapp, C.; Mews, R. *Eur. J. Inorg. Chem.* **2005**, 3536-3542.